

Article

Minimization of Voltage Harmonic Distortion of Synchronous Generators under Non-Linear Loading via Modulated Field Current

Oktay Karakaya ^{1,2,*} , Murat Erhan Balci ^{2,3} and Mehmet Hakan Hocaoglu ⁴ ¹ Department of Electronics Engineering, Gebze Technical University, Kocaeli 41400, Turkey² Department of R & D, ISBIR Electric Company, Balikesir 10150, Turkey³ Department of Electrical and Electronics Engineering, Balikesir University, Balikesir 10145, Turkey⁴ Department of Electrical and Electronics Engineering, Istanbul Ticaret University, Istanbul 34840, Turkey

* Correspondence: o.karakaya@gtu.edu.tr

Abstract: The synchronous generators (SGs) supplying non-linear loads have harmonically distorted terminal voltages. Hence, these distorted terminal voltages adversely affect the performance parameters of the supplied loads such as the power factor, current distortion, losses, and efficiency. To mitigate the harmonic voltages and currents, passive and active filters are generally employed. However, passive filters cause resonance problems, while active filters can cause high costs. On the other hand, in several recent studies to reduce the SG's terminal voltage harmonic distortion, which depends on the constructional design under the no-loading condition, the conventional DC excitation current has been modulated with AC harmonic components. These field current modulation methods have high computational complexity, and require extra hardware for their implementation. In the present paper, firstly, for the reduction of the terminal voltage harmonic distortion of the SG under non-linear loading conditions, the validity of the field current modulation technique is investigated. The numerical results show that by using the field current modulation method, under rated loading conditions, the total harmonic distortion of the terminal voltage can be reduced from 18% to 11%. Secondly, to provide a computational efficient and low-cost tool for optimal field current modulation, which minimizes the terminal voltage harmonic distortion, an Artificial Neural Network (ANN)-based model is proposed. Finally, with the integration of ANSYS Maxwell, ANSYS Simplorer, and MATLAB/Simulink software, the implementation of the developed model is demonstrated for the construction of the optimally modulated field current.

Keywords: synchronous generator; excitation current; harmonic distortion; artificial neural networks; data based on finite elements; harmonic elimination; harmonic compensation; non-linear loading



Citation: Karakaya, O.; Balci, M.E.; Hocaoglu, M.H. Minimization of Voltage Harmonic Distortion of Synchronous Generators under Non-Linear Loading via Modulated Field Current. *Energies* **2023**, *16*, 1789. <https://doi.org/10.3390/en16041789>

Academic Editors: Juan-José González de la Rosa, Sara Sulis and Olivia Florencias-Oliveros

Received: 17 January 2023

Revised: 7 February 2023

Accepted: 8 February 2023

Published: 10 February 2023



Copyright: © 2023 by the authors. Licensee MDPI, Basel, Switzerland. This article is an open access article distributed under the terms and conditions of the Creative Commons Attribution (CC BY) license (<https://creativecommons.org/licenses/by/4.0/>).

1. Introduction

Non-sinusoidal or distorted current characteristics exist in power system equipment such as lighting appliances, saturated electric machines, loads and generation units with power electronic interfaces, arc furnaces, welding machines, and high-voltage direct current (HVDC) transmission systems [1,2]. The distorted currents result in distorted voltage drops on the lines, thus leading to distorted bus voltages in the systems. Harmonically distorted voltages and currents have various adverse effects on power system components and loads. They can be specified as a decrease in power factor, the occurrence of frequency-related extra losses in the power system components and electrical machines, the shortening of the expected life of power system equipment, torque oscillations in rotating electric machines, malfunctions of protection, measurement, and control circuits, and resonance events in the system [3–5]. In particular, for electric machines, the winding losses may be significantly increased by high-order harmonic components of load currents while their cores can be saturated due to sub-harmonic or DC voltages [6–8].

1.1. Literature Review

Harmonic mitigation devices, such as passive [9] and active [2,10,11] filters, are commonly used in practice to reduce harmonic pollution in systems [5]. However, passive filters cause resonance problems, while active filters can cause high costs [12,13].

Thus, in [14,15], synchronous generators (SGs) were considered as electromechanical active harmonic filters, which have a lower cost when compared to active harmonic filters.

On the other hand, advanced control algorithms have been implemented to mitigate the current harmonic distortion of modern renewable-based distributed generation units under non-linear loading [16].

Furthermore, some studies focus on harmonic distortion mitigation by taking design aspects of SGs into account. As a result, their pole shapes, damper bar positions and numbers [17–23], and winding distributions [24–27] were optimized to reduce the SGs' voltage harmonic distortion.

Additionally, in [28], in order to reduce the terminal voltage total harmonic distortion of SGs, the field current profile was modified using the field reconstruction method (FRM). With the FRM, in the time domain, terminal voltages were simulated as a function of stator and rotor magnetic field, stator and field excitation (rotor) currents, and rotor positions. The analysis results were considered to determine the optimal profile of the field current under no-loading conditions. The method presented in [28] was also used for the dynamic simulation of non-salient and salient-pole SGs in the authors' later study [29].

In [30], by using simulation and experimental analysis for three-phase SGs, the modulation of the excitation field current was demonstrated as a tool to minimize specific harmonics of no-load phase voltages. The theoretical background of the study is based on the minimization of the airgap flux density, which is expressed as a function of the rotor magnetic field in the time domain. In the experimental system, for the modulation of the excitation field current, the fixed frequency band control is employed by using rotor position, airgap magnetic flux density, and field current measurement sensors.

1.2. Research Gap

The disadvantages of the two abovementioned field current modulation methods from [28,30] can be written as follows:

- They are based on time-domain expressions.
- Their implementation requires rotor position and magnetic flux density sensors in addition to the current measurement sensors.
- Due to first and second matters, they have high computational complexity and require extra hardware for their real-time implementation.

On the other hand, especially under non-linear loading, the harmonic interaction between the magnetic fields of the stator and rotor should be considered for the minimization of terminal voltage harmonic distortion. However, references [28,30] implemented the field current modulation for the reduction of the unloaded SG's terminal voltage harmonic distortion. Therefore, there is a need to show the validity of the field current modulation on the mitigation of the SG's terminal voltage harmonic distortion under non-linear loading conditions.

1.3. Motivation

In the present paper, firstly, for the reduction of the terminal voltage harmonic distortion of the SG under non-linear loading conditions, the validity of the field current modulation technique will be investigated.

Secondly, by considering the non-linear loading conditions of the SGs, the aim was to develop an ANN-based computationally efficient tool to determine the optimal modulation of the field current, which minimizes the terminal voltage harmonic distortion. It should be noted that the implementation of the developed tool will not require extra hardware such as rotor position and magnetic flux density sensors when compared to the other tools utilized in [28,30].

1.4. Contributions to the Knowledge

This paper's contributions to the knowledge are as follows:

- For the SGs dedicated to supplying non-linear loads, the performance of the field current modulation technique is analyzed for the reduction in the terminal voltage harmonic distortion. To this end, in the ANSYS Maxwell finite element (FE) analysis environment, by superimposing AC current components with various frequencies, magnitudes, and angles on the DC component, numerous field currents are modulated for the excitation of a three-phase salient-pole SG under non-linear loading. In the simulations, several loading levels are also taken into account.
- An ANN model is developed to express terminal voltages' harmonics in terms of the modulated field current's harmonic components and the loading level.
- In the ANSYS Maxwell and MATLAB/Simulink environments, the developed model is implemented as a computationally efficient tool to modulate the optimal field current of the SG. In the implementation, the minimization of the terminal voltage harmonic distortion under non-linear loading conditions is considered as an objective.

To provide the abovementioned contributions, the methodology presented in Figure 1 is applied in this study.

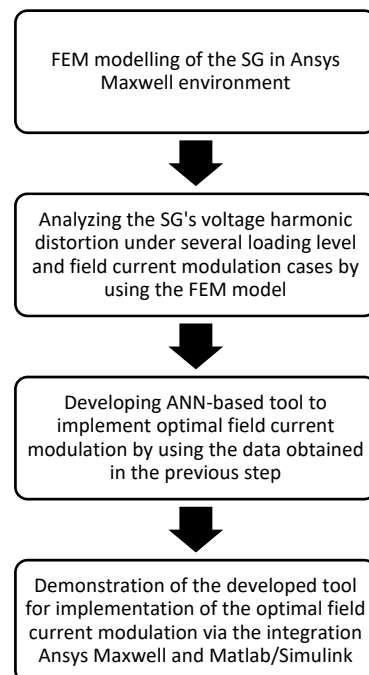


Figure 1. Methodology applied in this study.

1.5. Organization

The content of this paper is as follows: Section 2 models a three-phase SG in the ANSYS Maxwell environment, one of the most widely used FE analysis software packages. Section 3 evaluates the harmonic behavior of the modeled SG under modulated excitation current conditions. Section 4 presents the proposed ANN-based model. Section 5 interprets the implementation of the proposed model in practice, and Section 6 briefly presents the conclusions of the study.

2. Modeling of SG in Ansys Maxwell

In this section, to analyze the harmonic behavior of the terminal voltages of the three-phase salient-pole SGs under non-linear loading and modulated excitation current conditions, its 2D FE model is created in the ANSYS Maxwell environment. It should be noted that due to its high accuracy, the FE model has been widely employed in the design

and analysis of electric machines in the literature [31,32]. In addition, it can clearly be concluded from several studies [33,34] that the FEM and experimental results are very close to each other for SGs.

In addition, the model presented in this section is also used to provide data required for ANN modeling of the relationship between the harmonic components of the terminal voltages and the modulated excitation current. The rated values and design parameters of the considered three-phase SG are given in Table 1. In the analysis, it is loaded by a six-pulse uncontrolled rectifier supplying a resistor. Note that the considered load is one of the most widely employed non-linear loads in modern power systems [35,36].

Table 1. Parameters of the studied machine.

Parameter	Values
Rated power	538 kVA
Rated voltage	400 V
Rated frequency	50 Hz
Rotor type	Salient pole
Number of poles	6

To reduce the simulation time, simulation results are obtained for 1/6 of the model geometry given in Figure 2a. Note that for proper analysis sensitivity, the number of meshes is automatically determined as 1428 by ANSYS Maxwell. The load model is coupled with the 2D FE model of the SG through the Maxwell Circuit Editor (see Figure 2b). The PC used for the simulations has a 12-core Ryzen 9 3900x processor and 32 GB of RAM. Using this PC hardware, each simulation is run in 21.5 min.

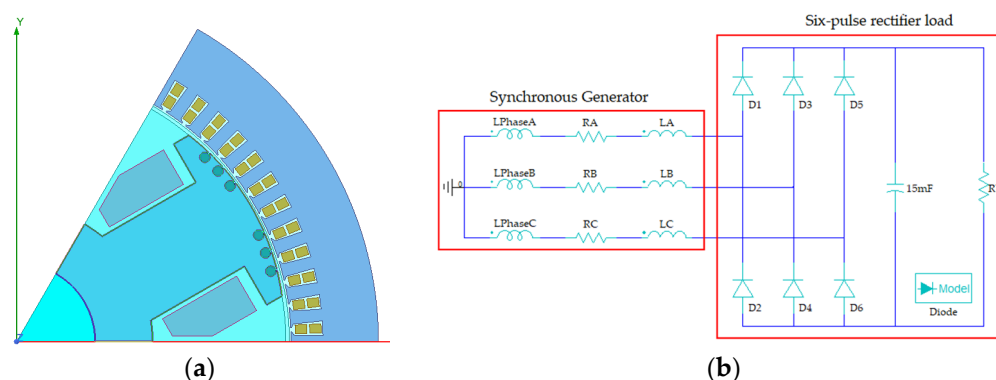


Figure 2. (a) Two-dimensional FE model of synchronous generator. (b) Coupling SG and load models within Maxwell Circuit Editor.

For the modeled system, the terminal voltage harmonic spectrum of the SG under no-load and rated loading conditions is plotted in Figures 3 and 4, respectively. V_h/V_1 (%) and I_h/I_1 (%) in these figures are the magnitudes of the harmonic components of the voltage and current expressed as a percentage, respectively. Figure 4 also presents the phase current harmonic spectrum of the SG under-rated loading case. Figure 3 shows that the terminal voltages have 5th and 7th harmonic orders for the no-load case. It is seen from Figure 4 that the current distortion of the six-pulse rectifier significantly affects the distortion of the terminal voltages, and their dominant harmonic orders turn into 5th, 7th, 11th, and 13th. For these two loading cases, the total harmonic distortion of the terminal voltage (THD_V) is found to be approximately 3.5% and 18%, respectively. In Equations (1) and (2), the expressions of the voltage total harmonic distortion (THD_V) and current total harmonic distortion (THD_I) indices are given.

$$THD_V = \frac{\sqrt{\sum_{h=2}^{50} V_h^2}}{V_1} \quad (1)$$

$$THD_I = \frac{\sqrt{\sum_{h=2}^{50} I_h^2}}{I_1}, \quad (2)$$

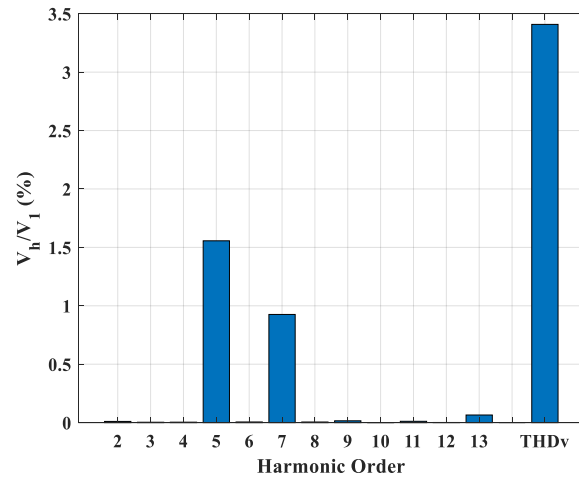


Figure 3. Terminal voltage harmonic spectrum of the SG under the no-loading condition.

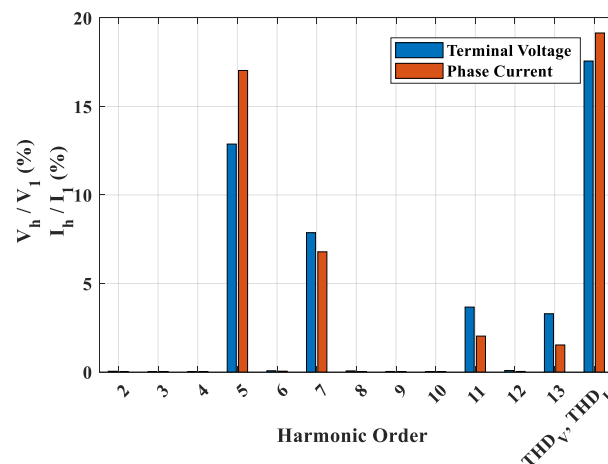


Figure 4. Terminal voltage and phase current harmonic spectrum of the SG under the rated loading condition.

In both equations, V_h and I_h stand for the magnitudes of the h th harmonic voltage and h th harmonic current, and V_1 and I_1 denote the magnitudes of the fundamental harmonic voltage and fundamental harmonic current, respectively.

3. Harmonic Behavior Analysis of SG under Modulated Field Current Conditions

In this section, by using the FE model presented in the previous section, the aim is to analyze the effect of the modulation of the field current on the terminal voltage harmonic distortion under different non-linear loading conditions. As mentioned before, the numerical results obtained in the analysis will also be used as data for developing the ANN model of the SG.

To this end, by using the modeled system, the field current is modulated by superimposing a single h th harmonic current component to the DC component. Accordingly, the expression of the current applied to the field winding can be written as:

$$i_f(t) = I_{f_{dc}} + \sqrt{2} \cdot I_{fh} \cdot \sin(2 \cdot \pi \cdot f_h \cdot t + \alpha_h) \quad (3)$$

where I_{fdc} denotes the DC component’s magnitude, I_{fh} , is the RMS value of the h th harmonic AC component in percent of the magnitude of the I_{fdc} , and f_h and α_h stand for frequency and phase angle of the h th harmonic AC component, respectively.

All three parameters of the h th harmonic AC component, I_{fh} , f_h , and α_h , can affect the airgap magnetic flux or terminal voltages. Hence, in the parametric analysis, they are taken into account. With 5° increment steps, α_h is varied from 0° to 355° . On the other hand, in the proposed method, the aim is to reduce the especially dominant harmonic components of the terminal voltage with an acceptable increase in field winding losses. For the analysis, the maximum values of I_{fh} and f_h are limited to 30% and 900 Hz, respectively. In addition, due to the fact that the terminal voltages vary under different loading conditions, the loading level should be considered as the fourth parameter in the analysis. The loading level term (LL) can be expressed as the ratio of the supplied load’s true apparent power (S_L) to the SG’s rated power (S_R):

$$LL(\%) = \frac{S_L}{S_R} 100 \tag{4}$$

where S_L is calculated in terms of true rms values of line voltages (V_{LL}) and currents (I_L):

$$S_L = \sqrt{3}V_L I_L = \sqrt{3} \sqrt{\sum_{h=1}^{50} V_h^2} \sqrt{\sum_{h=1}^{50} I_h^2} \tag{5}$$

As a result, for 19,440 cases of the four parameters mentioned above, the simulation results are obtained via the 2D FE model of the SG.

Thus, for the pure DC excitation and the various excitation currents modulated as an AC harmonic current superimposed on that of the DC, the terminal voltages are simulated. In the simulations, for the modulated excitation currents, the magnitude and angle of the harmonic component are varied. Then, the minimum THD_V values are determined for each modulated field current case. Accordingly, under low (25%), medium (50%), and full (100%) loading levels, the THD_V value for the pure DC excitation current and the minimum THD_V values for the modulated field current cases are presented in Figure 5.

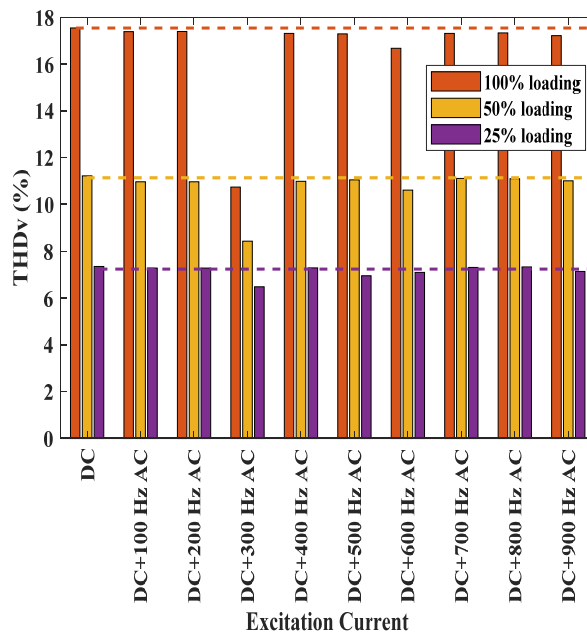


Figure 5. Lowest THD_V values obtained for the tested excitation currents.

It can be observed from Figure 5 that for all three loading levels, the minimum THD_V values are achieved by modulating the 6th harmonic current (300 Hz) and the DC current. Under 25%, 50%, and 100% loading ratios for the conventional pure DC field current,

the THD_V values for pure DC excitation are 8%, 12%, and 18%, respectively. Under the respective loading ratios, for the optimally modulated field current, the minimum THD_V values are seen as 6%, 8%, and 11%. Thus, it can be seen from these results that, especially for high loading levels, the modulation of the field current can achieve a considerable reduction in THD_V . On the other hand, under the respective loading levels, field current modulation with the 12th harmonic current (600 Hz) and DC components causes THD_V values of 7%, 11% and 17%. However, the other modulated field current cases do not considerably mitigate THD_V .

Here, to detail the behavior of the terminal voltages' distortion for the field current modulation with the 6th harmonic current (300 Hz) and DC components, the THD_V variations are plotted in terms of the magnitude and phase angle of the harmonic component under the considered loading levels (see Figure 6). Figure 6 clearly shows that for the achieved minimum THD_V values under three loading levels, such as 100%, 50% and 25%, the optimal values of the harmonic current's phase angle are 180° , 255° , and 315° , respectively. Accordingly, it can be posited that for the considered non-linear load, the optimal phase angle of the harmonic current added to DC field current varies between 180° and 360° with the decrement of the loading level. For the same objective, under the respective loading levels, the optimal magnitudes of the harmonic component are 20%, 15%, and 10% of the DC component. This means that there is a direct proportional relation between the optimal magnitude of the harmonic current and the loading level.

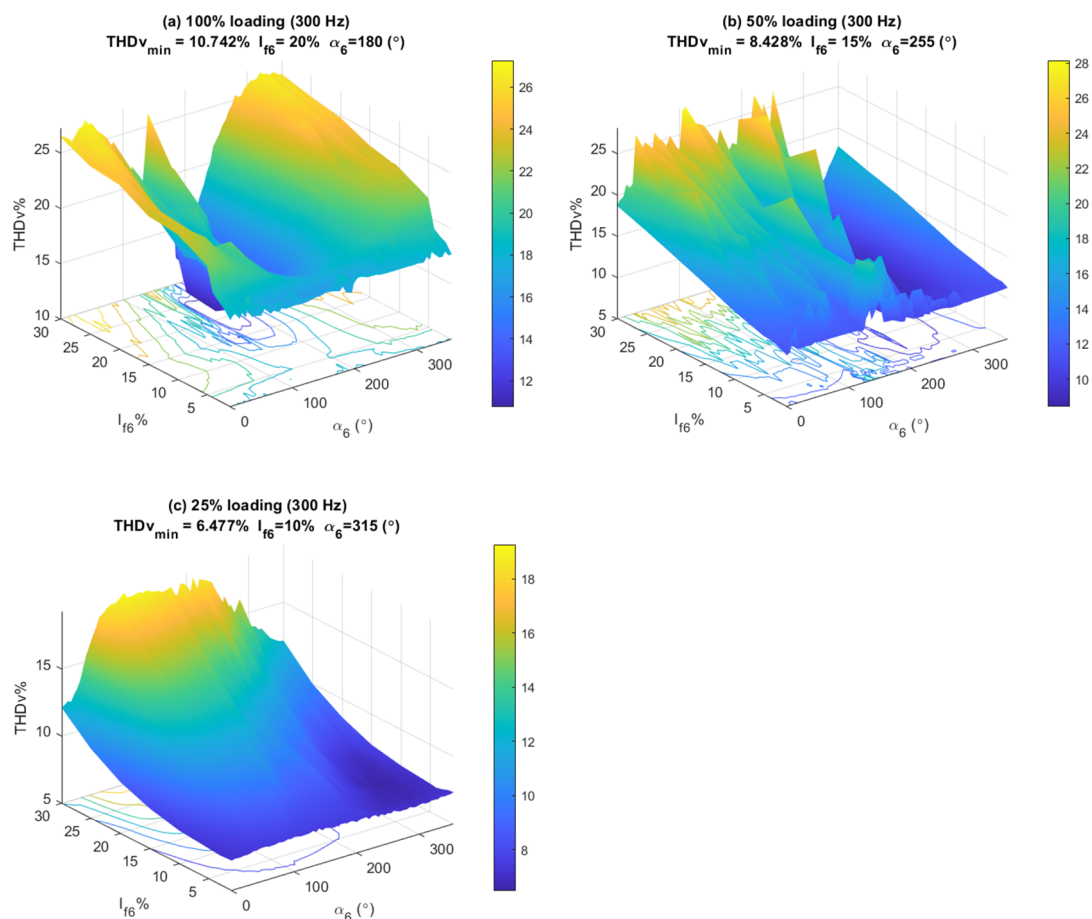


Figure 6. Surface plots of THD_V values in terms of magnitudes and phase angles of AC component with 300 Hz frequency (6th harmonic) under (a) 100%, (b) 50%, and (c) 25% loading conditions.

Regarding the analysis results detailed so far, it can be concluded that in order to minimize the harmonic distortion of the terminal voltages under different loading levels,

the excitation current can optimally be synthesized by adjusting the magnitude and phase angle of the 6th harmonic current component superimposed on the DC component.

Accordingly, in the next section, an ANN-based SG model is proposed as a tool to determine the optimally modulated excitation current by regarding the minimization of the individual or total voltage harmonic distortion as objectives.

4. Proposed ANN-Based Model

ANN-based models were considered to model the non-linear behavior of electrical machines in the literature [37–41]. Thus, in this paper, the ANN method is preferred to express the magnitudes and phase angles of the terminal voltage harmonics in terms of the magnitude and phase angle of the 6th harmonic current component superimposed on the DC excitation current and the SG's loading ratio.

4.1. Structure

The structure of the ANN used for the study is given in Figure 7. It has three main parts: input, hidden, and output layers. The input parameters of the first layer are defined as the effective value (I_{fh}) and phase angle (α_h) of the 6th harmonic component superimposed on the DC field current and the loading ratio (lr) of the SG. In the third layer, the magnitudes and phase angles of the terminal harmonic phase voltages are defined as output parameters or targets.

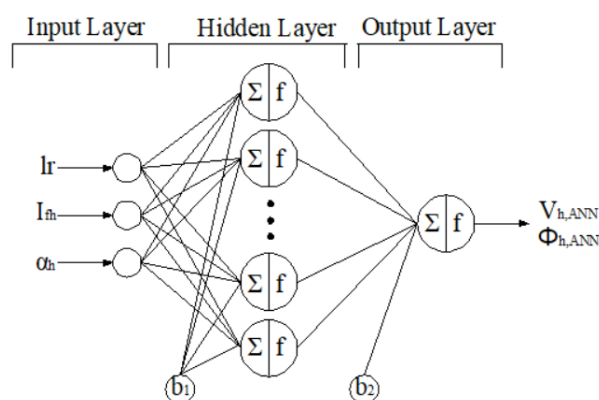


Figure 7. Structure of the used ANN.

The numbers of the data used for the training, testing, and validation of the ANN-based model are 1512, 324, and 324, respectively. Thus, a total of 2160 cases are simulated in the ANSYS Maxwell environment. The magnitudes and phase angles of the harmonic voltages are separately trained.

By performing numerous trial and error analyses, the proper network structure and learning algorithm are selected as the feedforward network structure with the Levenberg–Marquart learning algorithm. On the other hand, the hyperbolic tangent sigmoid transfer function (tansig) is used in the hidden and output layers.

A large number of neurons increases the accuracy of the model. However, this also increases the simulation time [42]. Due to this, regarding the performance and coefficient of determination, the numbers of neurons in the input, hidden, and output layers are properly determined as 3, 200, and 1, respectively.

As a measure of ANN performance over the training period, the mean-square-error (MSE) between the FE-based data and predicted data (ANN outputs) is calculated [43]:

$$E = \frac{1}{N} \sum_{i=1}^N (X_i - \hat{X}_i)^2 \quad (6)$$

In Equation (6), X_i and \hat{X}_i are the values of the magnitudes and phase angles of the harmonic voltages provided by FE analysis and their values estimated via ANN, respectively.

The ANN structure detailed here is developed in the MATLAB/Simulink environment. According to the structure shown in Figure 7, the relationship between the outputs and the input parameters can be written as in Equations (7) and (8).

$$V_{h,ANN} = \sum_{s=1}^S \left[lw_{(1,s)} \left(\frac{2}{1 + e^{(-2(\sum_{m=1}^M (iw_{(s,m)} (\frac{2}{1+e^{-2x(m)} - 1) + b_{1(s)}))} - 1))} - 1 \right) \right] + b_2 \quad (7)$$

$$\varphi_{h,ANN} = \sum_{s=1}^S \left[lw_{(1,s)} \left(\frac{2}{1 + e^{(-2(\sum_{m=1}^M (iw_{(s,m)} (\frac{2}{1+e^{-2x(m)} - 1) + b_{1(s)}))} - 1))} - 1 \right) \right] + b_2 \quad (8)$$

In Equations (7) and (8), iw is the weight matrix between the input and the hidden layers, and lw is the weight matrix between the hidden and the output layers. Additionally, M and S are the numbers of neurons in the input and hidden layers, $V_{h,ANN}$ is the magnitude of the h th harmonic phase voltage, $\Phi_{h,ANN}$ is the phase angle of the h th harmonic phase voltage, and b_1 and b_2 are the bias of the hidden and output layers, respectively. Note that each of the harmonic components has been trained separately.

4.2. ANN Results

Here, the training, testing, and validation of the developed ANN-based model will be presented. Since the SG is simulated to supply the balanced load, the results achieved for all phase voltages are the same. In addition, due to the fact that the six-pulse rectifier load has odd-order harmonics, the phase voltages of the simulated SG has considerably higher odd-order harmonics as well. Thus, the results are plotted for only odd harmonic orders of a phase (phase A) voltage in Figures 8–10.

The results plotted in Figures 8–10 show that for the magnitudes and phase angles of the phase voltages at fundamental and non-fundamental harmonics, the ANN-based model closely follows the reference dataset obtained via the FE method.

It should be mentioned that for the training of the voltage harmonic magnitudes, the coefficient of determination is close to 1, and the performance index reaches 0.0194. Additionally, for the training of the voltage harmonic phase angles, these respective parameters are 0.9596 and 0.218. They clearly point out that the training of the ANN network has been successfully achieved. The MSE values of the ANN model are given in Table 2. It can be seen from this table that during the training period, the MSE values have an acceptable value.

Table 2. MSE values of the ANN.

Harmonic Order	MSE (Magnitude)	MSE (Phase Angle)
Fundamental	4.0361×10^{-3}	2.0774×10^{-3}
3rd	9.4757×10^{-3}	8.6762×10^{-3}
5th	0.0059	0.1683
7th	0.0022	0.0928
9th	0.0096	0.1442
11th	0.00494	0.1467
13th	0.0194	0.2182

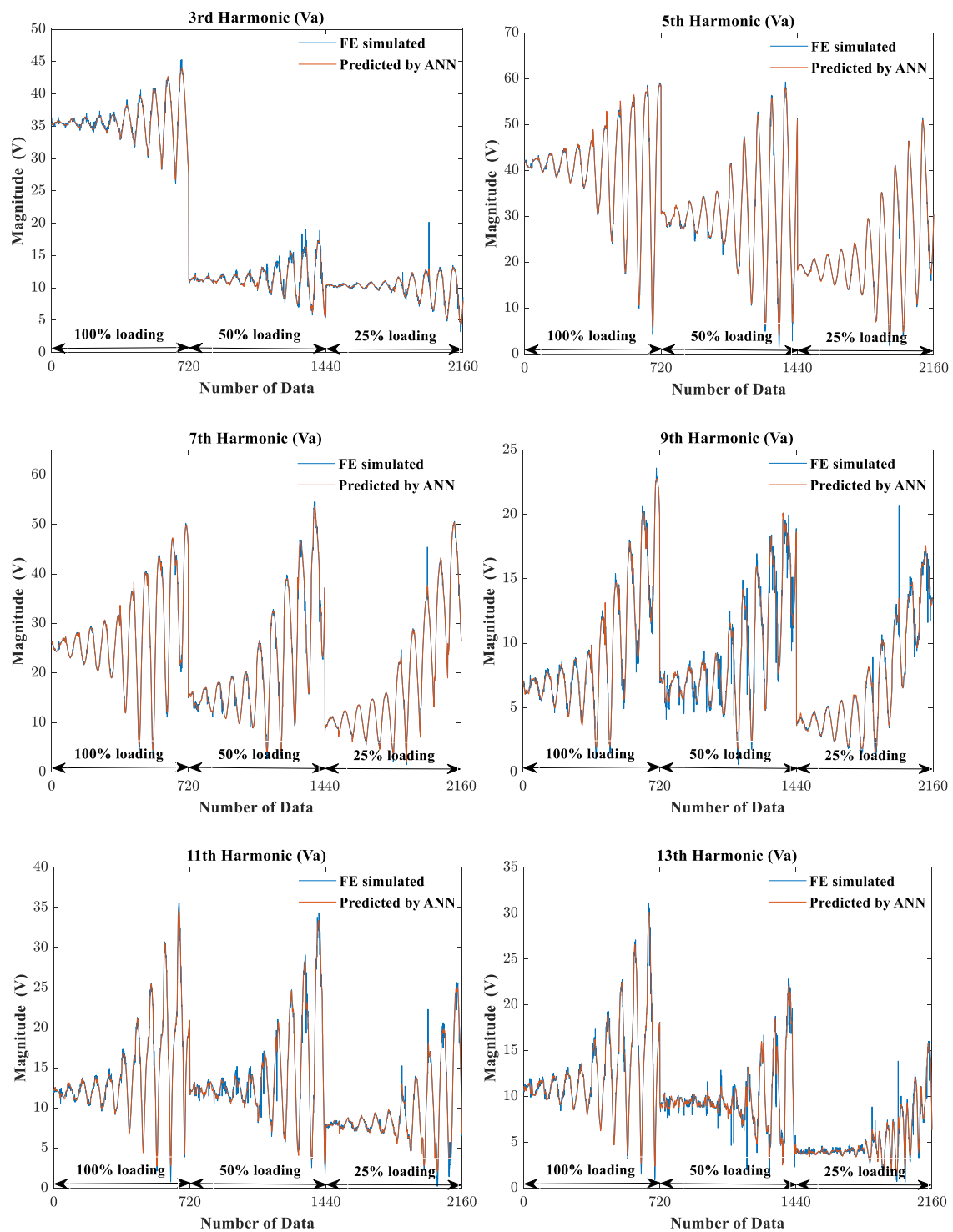


Figure 8. Magnitudes of the non-fundamental harmonic phase voltages simulated by FE and predicted by the developed ANN model.

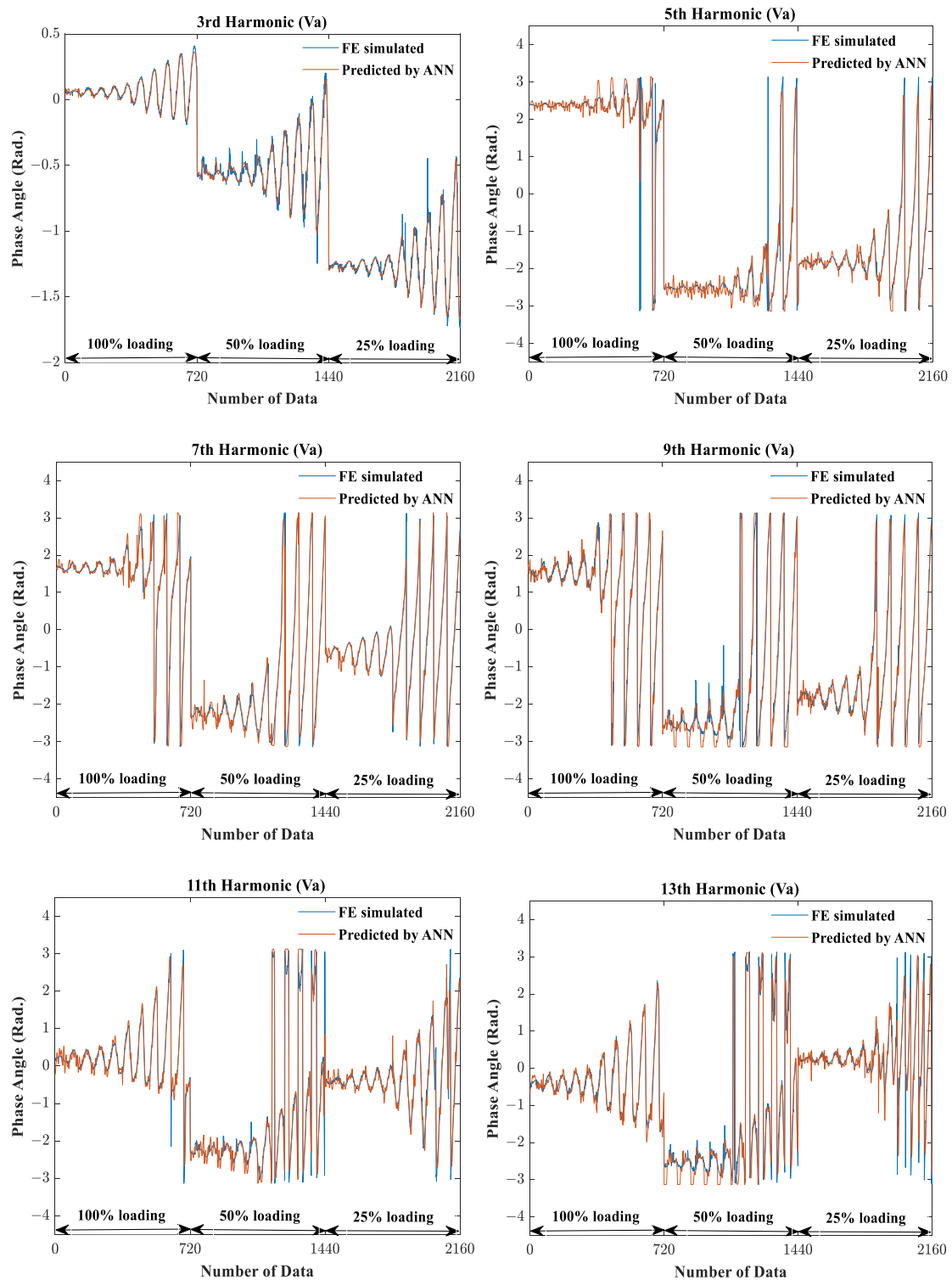


Figure 9. Phase angles of the non-fundamental harmonic phase voltages simulated by FE and predicted by the developed ANN model.

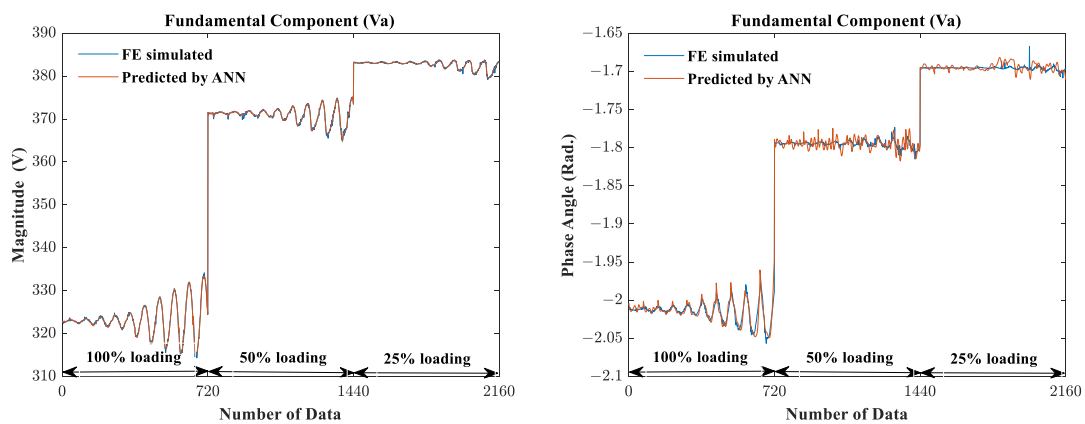


Figure 10. Magnitudes and phase angles of the fundamental harmonic phase voltages simulated by FE and predicted by the developed ANN model.

5. Implementation of the Proposed Model

In this section, for the modulation of the field current, the implementation of the suggested ANN-based model is demonstrated with the integration of MATLAB/Simulink, ANSYS Maxwell, and ANSYS SImplorer. In the simulated system, the FEM model of SG, which is created in ANSYS Maxwell, and the circuit of the six-pulse uncontrolled rectifier load are simulated in the ANSYS SImplorer environment (see Figure 11). Additionally, the modulation of the field current is optimally determined according to the ANN-based model provided in the MATLAB/Simulink environment (see Figure 12).

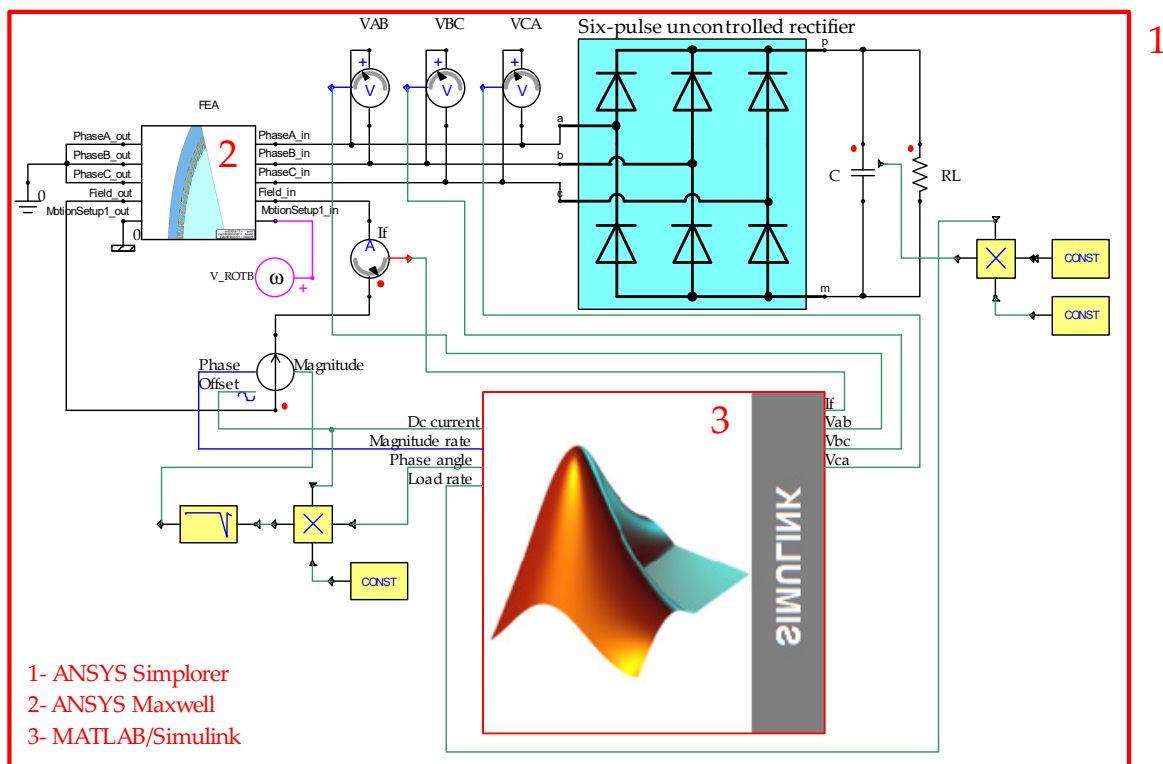


Figure 11. Test system created in ANSYS SImplorer.

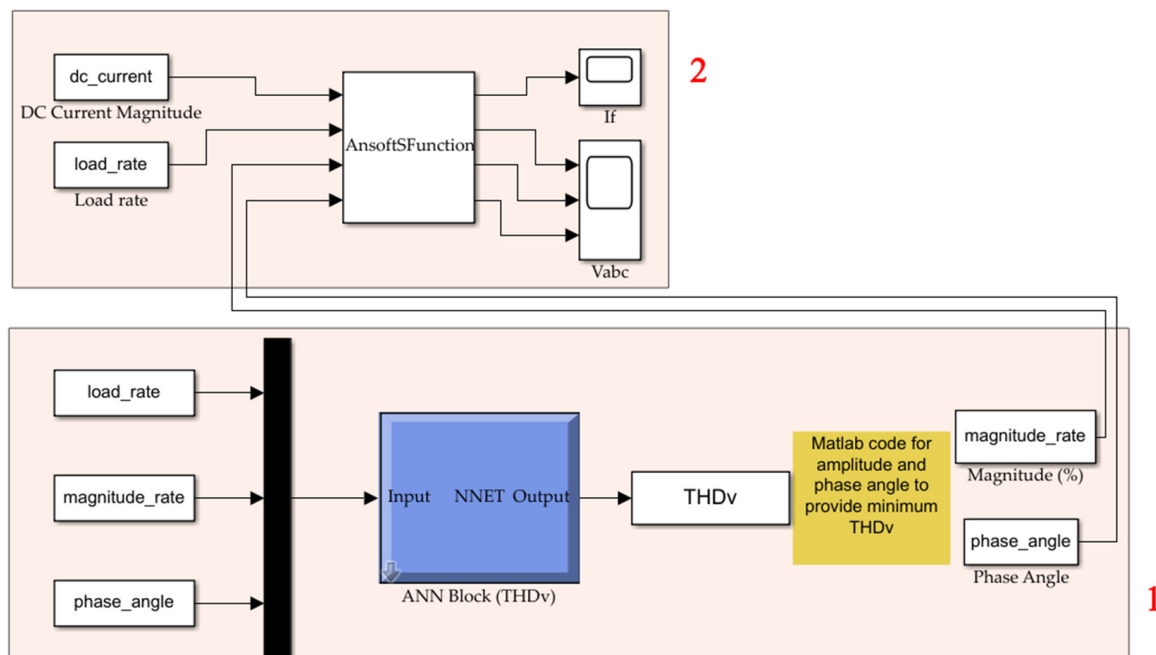


Figure 12. Implementation blocks of the proposed model in MATLAB/Simulink environment.

The determination blocks of the optimal field current created in the MATLAB/Simulink environment given in Figure 12 consist of two parts:

- In the first part (1), for the loading ratio of the SG, the code embedded in the block searches for the optimal magnitude and phase angle values of the 6th harmonic field current component, which should be superimposed on the DC field current.
- In the second part (2), the s-function block is used for data transition between ANSYS Simplorer and MATLAB/Simulink. It exports the optimal magnitude and phase angle values of the harmonic current component, which is obtained by the first part, to ANSYS Simplorer. It also exports the loading ratio data to ANSYS Simplorer.

Thus, by using the above detailed system, the optimally modulated field currents, which minimize THD_V , are injected into the field winding of the SG model in the ANSYS Maxwell 2D FE environment.

Under low (20%), semi (50%), full (100%), and over (120%) loading conditions, the individual and total harmonic distortions of the terminal line voltages, which are obtained for optimally modulated field current cases in ANSYS, are plotted in Figure 13. For the same conditions, the individual and total harmonic distortions of the terminal line voltages, which are predicted by the developed ANN-based model, are also presented in the same figure. It can be seen from Figure 13 that both models give almost the same results for the optimally modulated excitation conditions.

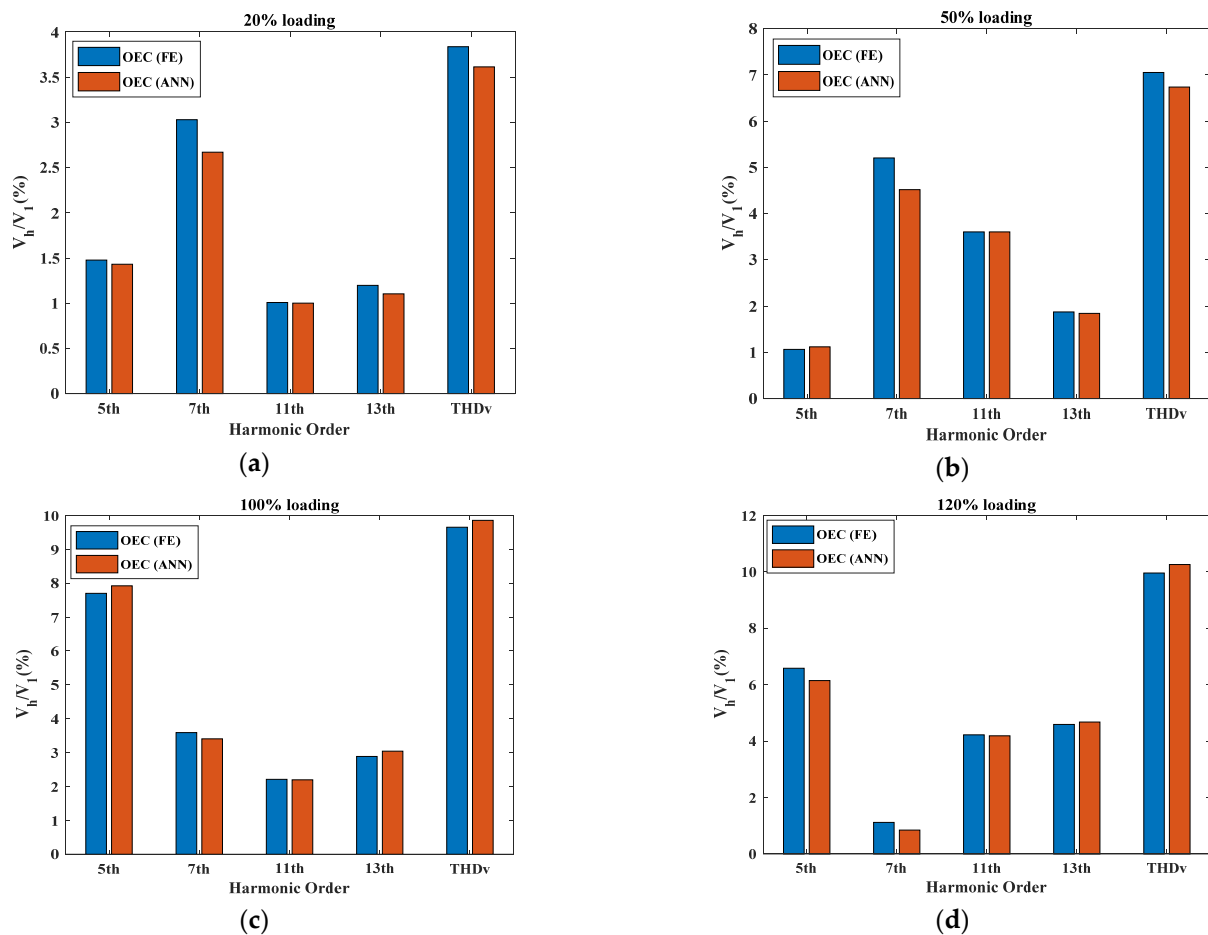


Figure 13. Individual and total harmonic distortions of the terminal line voltages obtained via the proposed (ANN) and FE model under (a) low (20%), (b) semi (50%), (c) full (100%) and (d) over (120%) loading levels for optimally modulated excitation current cases.

6. Conclusions

In this study, to investigate the terminal voltage harmonic distortion nature of the salient-pole SGs under several non-linear loading levels and modulated excitation current conditions, an extensive parametrical analysis is simulated by ANSYS Maxwell finite element (FE) analysis software.

In the analysis, a three-phase salient-pole SG is loaded by a six-pulse uncontrolled rectifier supplying a resistor, which is one of the most widely employed non-linear loads in modern power systems. Accordingly, for the conventional pure DC field current, it is seen from the analysis that the total harmonic distortion of terminal voltage (THD_V) of the SG's terminal voltage varies between 8% and 18% under the loading ratios from low (25%) to full loading conditions, respectively.

Additionally, in the simulations, by superimposing AC current components with various frequencies, magnitudes, and phase angles on the DC component, numerous field currents are modulated for the excitation of the SG under non-linear loading. Thus, the analysis results show that for the low and full loading ratios, the modulation of the field current from the sixth harmonic and the DC components reduces THD_V to 6% and 11%, respectively. This case clearly demonstrates that the terminal voltages of the SGs under non-linear loading can be effectively mitigated by the modulation of their field current.

The ANN-based SG model is recommended as a computationally efficient method to determine the optimal modulation of the field current, which minimizes the terminal voltage harmonic distortion. In the suggested model, terminal voltages' harmonics are expressed in terms of the modulated field current's harmonic components and the loading

level. It can be stated from the presented mean-squared error values that the ANN model sensitively estimates both the magnitudes and phase angles of the terminal voltages' individual harmonics.

Finally, with the integration of ANSYS Maxwell, ANSYS Simplorer, and MATLAB/Simulink software, the implementation of the suggested model is demonstrated for the construction of the optimally modulated field current. Thus, it is shown that the developed tool can successfully be employed for the minimization of the THD_V of the SG's terminal voltages based on the field current modulation strategy. Moreover, the authors will implement the ANN-based modulation tool to minimize the specific harmonics of the terminal voltages under non-linear loading conditions in their future work.

In this study, the proposed method is implemented by considering the SGs, which are dedicated to supply six-pulse uncontrolled rectifier loads. To improve the voltage's THD of the SGs under any non-linear load current profile using the proposed method, the data obtained from FEM for the respected load should be used to train the ANN model included in the proposed method.

The proposed method and various optimally designed passive filters will be comparatively evaluated with respect to their losses or energy efficiency in the authors' future work.

Author Contributions: Conceptualization: O.K., M.E.B. and M.H.H.; methodology: O.K., M.E.B. and M.H.H.; software: O.K.; validation: O.K.; formal analysis: O.K.; investigation: O.K.; resource: O.K.; writing—original draft, O.K.; writing—review & editing: M.E.B. and M.H.H.; visualization: O.K.; supervision: M.E.B. and M.H.H.; project administration: M.E.B. and M.H.H. All authors have read and agreed to the published version of the manuscript.

Funding: This research received no external funding.

Data Availability Statement: Not applicable.

Acknowledgments: We would like to thank ISBIR Electric Company Research & Development Department for giving us the opportunity to use its facilities and software.

Conflicts of Interest: The authors declare no conflict of interest.

Abbreviations

ANN	Artificial Neural Network
SG	Synchronous Generator
FE	Finite Element
FRM	Field Current Method

References

1. Michalec, Ł.; Jasiński, M.; Sikorski, T.; Leonowicz, Z.; Jasiński, Ł.; Suresh, V. Impact of Harmonic Currents of Nonlinear Loads on Power Quality of a Low Voltage Network—Review and Case Study. *Energies* **2021**, *14*, 3665. [[CrossRef](#)]
2. Buła, D.; Grabowski, D.; Maciążek, M. A review on optimization of active power filter placement and sizing methods. *Energies* **2022**, *15*, 1175. [[CrossRef](#)]
3. Wagner, V.E.; Balda, J.C.; Griffith, D.C.; McEachern, A.; Barnes, T.M.; Hartmann, D.P.; Phileggi, D.J.; Emmanuel, A.E.; Horton, W.F.; Reid, W.E. Effects of harmonics on equipment. *IEEE Trans. Power Deliv.* **1993**, *8*, 672–680. [[CrossRef](#)]
4. Singh, G.K. Power system harmonics research: A survey. *Eur. Trans. Electr. Power* **2009**, *19*, 151–172. [[CrossRef](#)]
5. Lumbreras, D.; Gálvez, E.; Collado, A.; Zaragoza, J. Trends in power quality, harmonic mitigation and standards for light and heavy industries: A review. *Energies* **2020**, *13*, 5792. [[CrossRef](#)]
6. Balci, M.E. Optimal C-type filter design to maximize transformer's loading capability under non-sinusoidal conditions. *Electr. Power Compon. Syst.* **2014**, *42*, 1565–1575. [[CrossRef](#)]
7. Arslan, E.; Sakar, S.; Balci, M.E. On the No-Load Loss of Power Transformers under Voltages with Sub-Harmonics. In Proceedings of the 2014 IEEE International Energy Conference (ENERGYCON), Cavtat, Croatia, 13–16 May 2014; IEEE: Piscataway, NJ, USA, 2014; pp. 228–233.
8. Canturk, S.; Balci, M.E.; Hocaoglu, M.H.; Koseoglu, A.K. Investigation of the Effects of DC Bias on Single-Phase Shell Type Transformers Using Frequency-Dependent Reluctance-Based Model. *IEEE Trans. Magn.* **2021**, *57*, 1–9. [[CrossRef](#)]
9. Karadeniz, A.; Balci, M.E. Comparative evaluation of common passive filter types regarding maximization of transformer's loading capability under non-sinusoidal conditions. *Electr. Power Syst. Res.* **2018**, *158*, 324–334. [[CrossRef](#)]

10. Ise, T.; Murakami, Y.; Tsuji, K. Charging and discharging characteristics of SMES with active filter in transmission system. *IEEE Trans. Magn.* **1987**, *23*, 545–548. [[CrossRef](#)]
11. Hoon, Y.; Mohd Radzi, M.A.; Hassan, M.K.; Mailah, N.F. Control algorithms of shunt active power filter for harmonics mitigation: A review. *Energies* **2017**, *10*, 2038. [[CrossRef](#)]
12. Das, J.C. Passive filters-potentialities and limitations. *IEEE Trans. Ind. Appl.* **2004**, *40*, 232–241. [[CrossRef](#)]
13. El-Habrouk, M.; Darwish, M.K.; Mehta, P. Active power filters: A review. *IEEE Proc.-Electr. Power Appl.* **2000**, *147*, 403–413. [[CrossRef](#)]
14. Abolhassani, M.T.; Toliyat, H.A.; Enjeti, P. An electromechanical active harmonic filter. In Proceedings of the IEMDC 2001, IEEE International Electric Machines and Drives Conference (Cat. No.01EX485), Cambridge, MA, USA, 17–20 June 2001; IEEE: Piscataway, NJ, USA, 2001; pp. 349–355.
15. Abolhassani, M.T.; Toliyat, H.A.; Enjeti, P. Harmonic compensation using advanced electric machines. In Proceedings of the IECON'01, 27th Annual Conference of the IEEE Industrial Electronics Society (Cat. No.37243), Denver, CO, USA, 29 November–2 December 2001; IEEE: Piscataway, NJ, USA, 2001; pp. 1388–1393.
16. Karadeniz, A.; Ozturk, O.; Koksoy, A.; Atsever, M.B.; Balci, M.E.; Hocaoglu, M.H. Accuracy assessment of frequency-domain models for harmonic analysis of residential type photovoltaic-distributed generation units. *Sol. Energy* **2022**, *233*, 182–195. [[CrossRef](#)]
17. Fan, Z.-N.; Han, L.; Liao, Y.; Xie, L.-D.; Wen, K.; Wang, J.; Dong, X.-C.; Yao, B. Effect of damper winding and stator slot skewing structure on no-load voltage waveform distortion and damper bar heat in large tubular hydro generator. *IEEE Access* **2018**, *6*, 22281–22291. [[CrossRef](#)]
18. Fan, Z.-n.; Liao, Y.; Han, L.; Xie, L.-D. No-load voltage waveform optimization and damper bars heat reduction of tubular hydrogenerator by different degree of adjusting damper bar pitch and skewing stator slot. *IEEE Trans. Energy Convers.* **2013**, *28*, 461–469. [[CrossRef](#)]
19. Nuzzo, S.; Degano, M.; Galea, M.; Gerada, C.; Gerada, D.; Brown, N. Improved damper cage design for salient-pole synchronous generators. *IEEE Trans. Ind. Electron.* **2016**, *64*, 1958–1970. [[CrossRef](#)]
20. Wang, Y.; Nuzzo, S.; Gerada, C.; Zhang, H.; Zhao, W.; Galea, M. Integrated Damper Cage for THD Improvements of Variable Speed Salient-Pole Synchronous Generators for the More Electric Aircraft. *IEEE Trans. Transp. Electr.* **2021**, *8*, 3618–3629. [[CrossRef](#)]
21. Perin, D.; Karaoglan, A.D.; Yilmaz, K. Using grey wolf optimizer to minimize voltage total harmonic distortion of a salient-pole synchronous generator. *Sci. Iran.* **2021**, 1–29. [[CrossRef](#)]
22. Karaoglan, A.D.; Perin, D. Rotor design optimization of a synchronous generator by considering the damper winding effect to minimize THD using grasshopper optimization algorithm. *Int. J. Optim. Control Theor. Appl. IJOCTA* **2022**, *12*, 90–98. [[CrossRef](#)]
23. Hyeon Myeong Woo, D.-H.L. Rotor Shape Design of the 10kVA Synchronous Winding Generator Based on Genetic Algorithm for Power THD Reduction. *Trans. Korean Inst. Electr. Eng.* **2021**, *70*, 1173–1180.
24. Gundogdu, T.; Komurgoz, G. Implementation of fractional slot concentrated winding technique to large salient-pole synchronous generators & development with permanent magnets. *Electr. Power Syst. Res.* **2013**, *105*, 57–70.
25. Dajaku, G.; Xie, W.; Gerling, D. Reduction of low space harmonics for the fractional slot concentrated windings using a novel stator design. *IEEE Trans. Magn.* **2013**, *50*, 1–12. [[CrossRef](#)]
26. Abdel-Khalik, A.S.; Ahmed, S.; Massoud, A.M. Low space harmonics cancelation in double-layer fractional slot winding using dual multiphase winding. *IEEE Trans. Magn.* **2014**, *51*, 1–10. [[CrossRef](#)]
27. Bekka, N.; Zaim, M.E.H.; Bernard, N.; Trichet, D. A novel methodology for optimal design of fractional slot with concentrated windings. *IEEE Trans. Energy Convers.* **2016**, *31*, 1153–1160. [[CrossRef](#)]
28. Kimpara, M.L.M.; Pinto, J.O.P.; Fahimi, B.; Ribeiro, P.; Godoy, R.B.; Silva, L.E.B. Field reconstruction method applied for harmonic voltage mitigation in salient pole synchronous generators. In Proceedings of the 2013 Brazilian Power Electronics Conference, Gramado, Brazil, 27–31 October 2013; IEEE: Piscataway, NJ, USA, 2013; pp. 890–895.
29. Kimpara, M.L.M.; Godoy, R.B.; Ribeiro, P.E.M.; da Silva, L.E.B.; Fahimi, B.; Pinto, J.O.P. A new synchronous machine modeling using the field reconstruction method. *J. Control Autom. Electr. Syst.* **2014**, *25*, 481–492. [[CrossRef](#)]
30. Evestedt, F.; Pérez-Loya, J.J.; Abrahamsson, C.J.D.; Lundin, U. Controlling airgap magnetic flux density harmonics in synchronous machines using field current injection. *Electr. Eng.* **2021**, *103*, 195–203. [[CrossRef](#)]
31. Lei, G.; Zhu, J.; Guo, Y.; Liu, C.; Ma, B. A review of design optimization methods for electrical machines. *Energies* **2017**, *10*, 1962. [[CrossRef](#)]
32. Liu, C.; Chau, K.T.; Lee, C.H.T.; Song, Z. A critical review of advanced electric machines and control strategies for electric vehicles. *Proc. IEEE* **2020**, *109*, 1004–1028. [[CrossRef](#)]
33. Nuzzo, S.; Galea, M.; Gerada, C.; Brown, N. A fast method for modeling skew and its effects in salient-pole synchronous generators. *IEEE Trans. Ind. Electron.* **2017**, *64*, 7679–7688. [[CrossRef](#)]
34. Zhan, Y.; Kong, K.; Xu, G.; Kang, J.; Zhao, H. Analysis of damper transient currents in salient-pole synchronous generator with skewed armature slots considering interbar currents. *IEEE Trans. Ind. Appl.* **2018**, *55*, 336–343. [[CrossRef](#)]
35. Lian, K.L.; Perkins, B.K.; Lehn, P.W. Harmonic analysis of a three-phase diode bridge rectifier based on sampled-data model. *IEEE Trans. Power Deliv.* **2008**, *23*, 1088–1096. [[CrossRef](#)]

36. Arvindan, A.N.; Abinaya, B. THD Mitigation in line currents of 6-pulse diode bridge rectifier using the delta-Wye transformer as a triplen harmonic filter. *Proc. NPSC* **2010**, *10*, 210–215.
37. Hadjout, L.; Takorabet, N.; Ibtouen, R.; Mezani, S. Optimization of instantaneous torque shape of PM motors using artificial neural networks based on FE results. *IEEE Trans. Magn.* **2006**, *42*, 1283–1286. [[CrossRef](#)]
38. Wu, H.; Zhang, Y.; Fu, W.; Zhang, C.; Niu, S. A Novel Pre-Processing Method for Neural Network-Based Magnetic Field Approximation. *IEEE Trans. Magn.* **2021**, *57*, 1–9. [[CrossRef](#)]
39. Ibrahim, I.; Silva, R.; Mohammadi, M.H.; Ghorbanian, V.; Lowther, D.A. Surrogate-based acoustic noise prediction of electric motors. *IEEE Trans. Magn.* **2020**, *56*, 1–4. [[CrossRef](#)]
40. Tahkola, M.; Keränen, J.; Sedov, D.; Far, M.F.; Kortelainen, J. Surrogate modeling of electrical machine torque using artificial neural networks. *IEEE Access* **2020**, *8*, 220027–220045. [[CrossRef](#)]
41. Brescia, E.; Costantino, D.; Massenio, P.R.; Monopoli, V.G.; Cupertino, F.; Cascella, G.L. A Design Method for the Cogging Torque Minimization of Permanent Magnet Machines with a Segmented Stator Core Based on ANN Surrogate Models. *Energies* **2021**, *14*, 1880. [[CrossRef](#)]
42. da Silva, C.D.L.; Cardoso Junior, G.; Mariotto, L.; Marchesan, G. Phasor estimation in power systems using a neural network with online training for numerical relays purposes. *IET Sci. Meas. Technol.* **2015**, *9*, 836–841. [[CrossRef](#)]
43. Beale, M.H.; Hagan, M.T.; Demuth, H.B. Neural network toolbox. *User Guide MathWorks* **2010**, *2*, 77–81.

Disclaimer/Publisher’s Note: The statements, opinions and data contained in all publications are solely those of the individual author(s) and contributor(s) and not of MDPI and/or the editor(s). MDPI and/or the editor(s) disclaim responsibility for any injury to people or property resulting from any ideas, methods, instructions or products referred to in the content.